THE JOURNAL OF PHYSICAL CHEMISTRY C

Article

pubs.acs.org/JPCC

Graphitization of Graphene Oxide with Ethanol during Thermal Reduction

Cheng Gong,[†] Muge Acik,[†] Ramin M. Abolfath,[‡,∥] Yves Chabal,*[,†] and Kyeongjae Cho*[,†,§]

[†]Department of Materials Science and Engineering, The University of Texas at Dallas, Richardson, Texas 75080, United States

[‡]School of Natural Science and Mathematics, The University of Texas at Dallas, Richardson, Texas 75080, United States

[§]Department of Physics, The University of Texas at Dallas, Richardson, Texas 75080, United States

Supporting Information

ABSTRACT: As an atypical reductant, ethanol has recently been considered for reducing the oxygen concentration and restoring the graphitic structure in multilayered graphene oxide (GO) during annealing [Su et al., *ACS Nano* **2010**, *4*, 5285]. The reaction mechanism is, however, still not well understood, hindering progress in the use of GO. By combining density functional theory (DFT), ab initio molecular dynamics (MD) calculations, and in situ infrared absorption spectroscopy, the thermal evolution of both carbonyl and ether groups in multilayered GO is shown to vary dramatically upon individual intercalation of methanol, ethanol, and water molecules. In hydrated GO, bare etch holes are generated by thermal annealing, as evidenced by the evolution of carbon dioxide (CO_2) molecules. In contrast, the replacement of water by methanol or ethanol prevents defect enlargement during annealing. Furthermore, ethanol is found to repair the etch holes by facilitating the formation of new hexagonal carbon rings. Ab initio MD simulations map out the likely reaction pathways that are subsequently verified by DFT total energy calculations. The elucidation of the mechanism of etch hole healing in GO suggests new ways to tailor the structural and electronic properties of reduced GO (rGO) and graphene for a variety of applications requiring defect engineering.

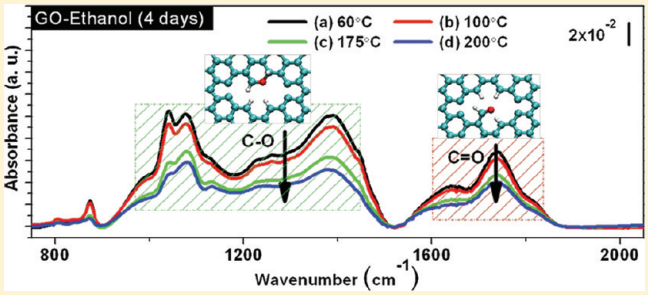

1. INTRODUCTION

Since the demonstration that individual graphene flakes can be prepared by mechanical exfoliation,[1] much effort has been devoted to producing large size and high-quality graphene sheets in large volume. Mechanical exfoliation of graphite is the most popular approach to obtain high-uniformity monolayer graphene flakes with a typical size of tens of micrometers. However, this approach is not scalable and consequently not amenable for mass production. Compared to the physical exfoliation methods, epitaxial growth and chemical exfoliation methods are preferable for large scale production. There are still substantial limitations associated with epitaxial growth methods. For instance, techniques for transferring graphene prepared from the thermal decomposition of silicon carbide[2] to other desirable dielectric substrates are not well developed. Graphene fabricated on transition metal substrates originating from either surface segregation[3] of carbon atoms dissolved in metal substrates or decomposition[4−6] of carbon-containing molecules on metal surfaces has also several limitations: (i) it is costly to produce; (ii) synthesized graphene is far from ideal (grain boundaries, ad-layers, and wrinkles); and (iii) it is expensive to dissolve the metal substrate and hard to transfer the graphene from a metal substrate to a target dielectric substrate. Consequently, it is challenging to develop epitaxial methods for mass production. As a result, wet oxidation of graphite followed by exfoliation and GO reduction[7] has been considered instead of these other synthesis techniques as a means to produce well-dispersed graphene flakes (i.e., rGO flakes) on a large scale.[8]

GO is a nonstoichiometric oxidized graphite having several in-plane oxygen-containing groups (i.e., derivatives of carbonyls, ethers, carboxyls, and hydroxyls) located at the sheet edges (boundary of flakes and edges of etch holes) and out-of-plane oxygen-containing groups (epoxides and hydroxyls) on the basal plane.[9−14] Two main approaches have been used in recent years for reducing GO: (1) chemical reduction and (2) thermal annealing. In the first case, strong reductants, such as anhydrous hydrazine,[15] hydrazine monohydrate,[16] sodium borohydride,[17,18] hydroquinone,[19] and vitamin C,[20] have been used to reduce GO, increasing the C/O ratio from 2:1[21] in as-made GO to approximately 15:1.[22] However, reduced graphene produced by the chemical reduction of exfoliated GO has poor electrical properties due to the presence of contaminants (e.g., reducing agents, oxygen-containing groups, or byproduct of reduction process) and structural defects.

An alternative route to chemical reduction is thermal annealing that involves reactions of neighboring oxygen-containing groups and with molecules intercalated between

Received: December 30, 2011
Revised: April 6, 2012
Published: April 18, 2012

the GO planes, providing reaction products such as H_2O, CO_2, and CO molecules. In most experimental studies, chemical reduction and thermal annealing are used simultaneously[23] to optimize the reduction efficiency and reach a C/O ratio higher than 250:1.[24] Thermal annealing, although effective to remove oxygen species, has two limitations to achieve an effective transformation from GO to high quality graphene: (1) in-plane carbonyl and ether groups are extraordinarily stable leftovers that are hard to remove even after annealing at high temperatures; and (2) etch holes are formed or enlarged (evidenced by the release of CO_2 and CO molecules), so that the C═C sp^2 π-bond network is much more defective in rGO flakes. Therefore, besides simple oxygen removal by reduction of GO, enhancing the degree of graphitization (suppressing the damage and repairing the C═C sp^2 π-bond network at defect regions) is a practical way to further improve the electrical properties of exfoliated rGO sheets for nanoelectronics applications.

Alcohols have recently been considered as atypical reductants effective in the reduction[25] of GO and the restoration[26] of the graphitic structure. Despite detailed characterization studies (elemental composition analysis,[24] crystalline structure variation,[27] and electrical conductance measurements[26]), the detailed mechanisms are yet to be elucidated. It is therefore important to understand the role of alcohols and their interactions with rGO in terms of the specific chemical bonding configurations and the way that they incorporate into the network to restore the graphitic structure.

In this work, we combine in situ Fourier transform infrared (FTIR) spectroscopy, ab initio molecular dynamics simulations, and first-principles DFT calculations to uncover the mechanisms of oxygen removal and network modification (e.g., repair) during thermal annealing as a function of the solvent. FTIR measurements are performed in a relatively mild temperature range (~60−200 °C) on multilayered GO intercalated by methanol, ethanol, or water. Both ether and carbonyl groups are observed as components at etch holes during annealing, particularly in water ambient. In methanol, these components remain essentially constant. In contrast, ethanol in the interlayer of GO is found to effectively foster oxygen removal (e.g., of the carbonyls and ethers) and to repair the carbon matrix during annealing.

Ab initio molecular dynamics simulations are used to explore possible mechanisms involving carbon atom incorporation into the etch holes, which can take place when an alcohol molecule approaches a bare etch hole. We find that methanol intercalation in GO prevents the enlargement of etch holes (unlike water), maintaining an almost constant etch hole carbonyl/ether concentration (i.e., thermal stabilization of etch hole patches). Furthermore, ethanol intercalation results in a new carbon hexagonal ring formation, and the graphitic structure is gradually recovered with an associated decrease in etch hole carbonyl/ether concentration. The removal of oxygen is more efficient in the presence of ethanol than methanol intercalated in GO. This contrasts the chemical evolution of oxygen removal in thermally rGO (initially intercalated with water) by formation of etch hole carbonyls and enlargement of the etch hole, with an increased etch hole carbonyl/ether concentration. The formation of chemically reactive bare etch holes in rGO during the annealing process provides a platform for the decomposition of methanol or ethanol to graft the carbon species to the etch holes. In particular, we present an etch hole healing mechanism by ethanol to recover the graphitic structure and to improve the electrical properties of rGO.

2. MATERIALS AND METHODS

2.1. Synthesis of Graphene Oxide. Multilayered GO flakes were synthesized using the modified Hummers' method.[28,29] The starting material is commercially available graphite powder (SP-1 grade 325 mesh, Bay Carbon Inc.). The oxidation of the graphite powder is initiated by a pretreatment using potassium persulfate ($K_2S_2O_8$) and phosphorus pentoxide (P_2O_5) at 90 °C. Then, the pretreated partially oxidized graphite is further treated with potassium permanganate ($KMnO_4$) as an oxidant dispersed in an acid environment using H_2SO_4. For purification of as-synthesized GO, a prepared 2 wt % of aqueous GO dispersion was dialyzed in Snake Skin dialysis membranes using ultrapure Milli-Q water for at least two weeks until the pH of the solution was ~6−7. Then, a GO solution with a concentration of 0.18 mg/mL was prepared from dialyzed and dried GO flakes.

2.2. Substrate Preparation. Prior to deposition, the substrate (oxidized and double-side polished float-zone Si(100)) was mechanically cleaned by rubbing with a Q-tip soaked with ethyl acetate, ethanol, and deionized water (18 MΩ, Millipore). Organic residuals were removed from the substrate surface by immersing the substrate in a piranha solution, a mixture of H_2SO_4 and H_2O_2 (2:1 vol %) maintained at 90 °C for 15 min.

2.3. Alcohol Intercalation Process. Prior to thermal annealing, 0.05 μL aliquots of the aqueous GO solution was further transferred on the mechanically cleaned SiO_2/Si substrates via direct drop casting and then dried in air on the substrates. Next, each multilayered GO sample on a SiO_2/Si substrate was soaked into 40 mL of methyl alcohol (i.e., methanol, 99.9%, Fisher Scientific, Certified ACS grade, 0.02 vol % of water) or ethyl alcohol (i.e., ethanol, 95%, 190 proof, Pharmco-AAPER, 5% of water) in a sealed centrifuge tube and kept closed. An exchange-alcohol technique was used to eliminate the intercalated water in the as-synthesized GO. The alcohol solution was replaced with fresh alcohol every day without any disturbance of the GO thin film on the SiO_2/Si substrates in solution. After blowing with dry nitrogen, each sample (initially soaked in alcohol) was directly transferred into the annealing chamber in less than a minute under laboratory humidity of 34−40% (dew point of 8.0−11.0).

2.4. Thermal Annealing Process and FTIR Measurements. Thermal annealing of these GO samples on SiO_2/Si substrates was achieved by direct resistive heating of the Si substrates, using two tantalum clips in an evacuated chamber placed in the IR sample compartment of a spectrometer. The IR beam was incident on the surface close to the Brewster's angle (~70°). The temperature was monitored by a K-type thermocouple spot-welded to a Ta clip attached to the sample edge. In this arrangement, the thermocouple reads lower by ~20−50 °C, as calibrated with a pyrometer. Therefore, the errors are systematic, and temperature *changes* can be recorded reproducibly.

The sample was placed in the IR sample compartment with the IR beam aligned at the Brewster's angle (~70°) for direct transmission. During in situ FTIR measurements, the annealing chamber was kept in vacuum (10^{-3}−10^{-4} Torr) and the sample at 60 °C, after each specific annealing cycle, with no exposure to air. The spectrometer itself was purged with nitrogen. The annealing cycles consisted in holding the sample for 5 min at

dx.doi.org/10.1021/jp212584t | J. Phys. Chem. C 2012, 116, 9969−9979

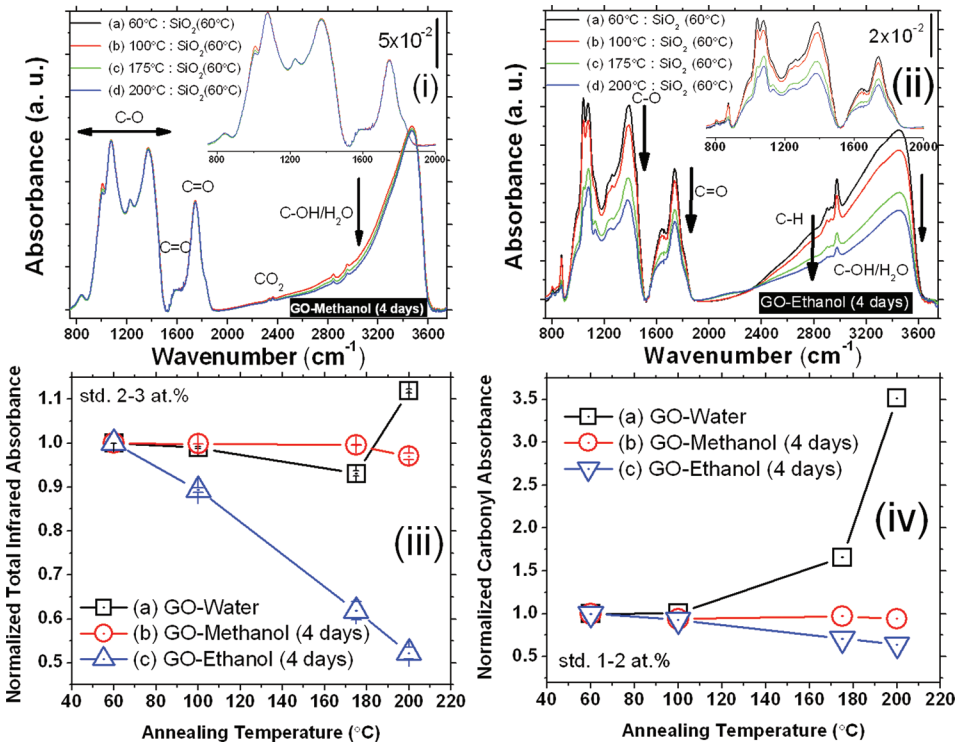

Figure 1. Infrared transmission absorbance spectra of GO intercalated with methanol (i) or ethanol (ii) after a 4-day exchange and integrated oxygen concentration as a function of annealing temperatures (iii,iv). Absorbance spectra are given after annealing at (a) 60−100 °C, (b) 100−175 °C, and (c) 175−200 °C. (iii) Normalized total infrared absorbance is calculated from integrations of total absorbance under each spectrum at 400−4000 cm^{-1} by normalization to the initial total oxygen concentration. (iv) Normalized carbonyl absorbance calculated at 1500−1850 cm^{-1} by normalization to the initial total oxygen concentration given for GO intercalated with (a) water, (b) methanol, and (c) ethanol.

each annealing temperature, and the total annealing time for the overall experiments per sample was approximately 8 h. Sample flaking at high temperature limited the experiments to a maximum annealing temperature of 200 °C.

2.5. Molecular Dynamics Calculations. Ab initio MD implemented in a Vienna ab initio simulation package (VASP)[30] was used as the main computational tool for all the MD simulations in this work. For the density functional theory (DFT) total energy calculations at each atomic configuration, projector-augmented wave (PAW)[31] potentials were used to describe the ionic cores. The generalized gradient approximation (GGA) proposed by Perdew, Burke, and Ernzerhof (PBE)[32] was used for exchange and correlation functional. For the wave function expansion, a plane wave basis was used with cutoff energy of 400 eV.

The current MD calculations are checked against previous DFT calculations,[33] by examining the consistency of the ab initio MD description of the proposed chemical reactions with previous experimental and DFT results (i.e., the interaction between a bare etch hole and H_2O discussed in ref 33 is reproduced by MD calculations in Figure 2a,b). The size of the graphene supercell is 2.13 nm × 1.97 nm for the ab initio MD simulations. Eight neighboring carbon atoms are removed to form a bare etch hole (Figure 2a,c,f). As discussed before, a number of neighboring carbon dangling bonds may not be formed simultaneously but result from several chemical reactions of neighboring oxygen functionalities. Therefore, a bare-etch-hole model assuming the removal of eight neighboring carbon atoms is adopted to explore the interaction of alcohol molecules. Periodic boundary conditions are applied along the graphene basal plane in both *x*- and *y*-directions to avoid any edge effect. A ∼12 Å vacuum region is applied perpendicular to the graphene basal plane. The simulations are performed in a canonical ensemble mode (NVT) with a Nose−Hoover thermostat for temperature control. A small time step of 0.2 fs is used to fully describe the details of fast chemical reactions, and the total simulation time spans are 1−2 ps.

2.6. Density Functional Theory Calculations. To investigate the energy of initial, intermediate, and final structures of various reactions, DFT total energy calculations were carried out within VASP, using the same PAW potentials and PBE-GGA functional used in the ab initio MD calculations for consistency. For all energy calculations of chemical reactions (Figures 3 and 6), the same supercell model as the ab initio MD simulation supercell was used. For the study of the migration of out-of-plane oxygen-containing groups on the graphene basal plane toward an etch hole, a smaller graphene supercell (1.23 nm × 1.70 nm) was used in which four neighboring carbon atoms are removed to form a smaller etch hole (Figure 5). The etch hole edge was decorated by either carbonyl or ether. Periodic boundary conditions were applied along the graphene basal plane, and the perpendicular distance to the periodic images was 12 Å to minimize the disturbance from neighboring image supercells.

3. RESULTS AND DISCUSSION

3.1. Formation of Etch Holes. The multilayered GO is known to trap water in the space between the GO layers, as the oxidized GO flakes settle during the synthesis steps performed in deionized water. Using in situ infrared spectroscopy in transmission mode, we have previously determined that the enlargement of reactive etch holes in thermally rGO results

dx.doi.org/10.1021/jp212584t | J. Phys. Chem. C 2012, 116, 9969−9979

from intercalated water reacting with carbon dangling bonds,[33] based on the observation of C−O and C═O species formation at the etch holes (see increased IR absorbance in Figure S1, Supporting Information). A singlet peak appearing at ∼2340 cm^{-1} (shown in the inset of IR spectra of Figure S1, Supporting Information) also indicates CO_2 production upon annealing to 200 °C, hence the removal of carbon. The formation of these etch holes have been also confirmed by high-resolution transmission electron microscopy (HRTEM).[9]

3.2. Accessibility of Bare Etch Holes by Intercalated Molecules. As they are formed by carbon removal, etch holes develop carbon dangling bonds that are the preferential adsorption sites for both epoxide and hydroxyl groups in the basal plane and intercalated molecules in close proximity. The migration of basal plane species to the edge of the etch hole is determined by their hopping barrier on the graphene basal plane. Li et al.[34] calculated with DFT that the hopping barrier for an isolated epoxide on the graphene basal plane is ∼0.9 eV. Our DFT calculations provide similar hopping barriers (0.5−0.8 eV) for hydroxyls and epoxides as shown in Figure 5. However, the diffusivity of methanol, ethanol, or water intercalated between GO layers is affected by the hydrogen bond network including epoxides and hydroxyls on GO. The strength of these hydrogen bonds (∼0.2 eV) is weaker than the activation barriers for the migration of epoxide/hydroxyl groups on the basal plane. When multilayered GO is intercalated by methanol, ethanol, or water, these intercalated molecules are in closer proximity or can approach the bare etch holes more efficiently (i.e., faster) than the pre-existing out-of-plane epoxide/hydroxyl groups, particularly when their concentration is high. Therefore, these intercalated molecules are expected to react at bare etch holes well before neighboring oxygen functionalities can migrate from the basal plane.

3.3. Experimental Evidence for the Thermal Reduction of GO Intercalated with Methanol. X-ray diffraction (XRD) measurements performed after immersion in methanol show a slight shift of interlayer spacing of GO (originally ∼8.88 Å with water intercalation) to 8.92 Å (Figure S2, Supporting Information), indicating that water has been replaced by methanol after 4 days of immersion. The reduction mechanism of rGO intercalated with either methanol or ethanol is then derived primarily from IR spectroscopy combined with in situ thermal annealing. Figure 1 shows that a 4-day methanol or ethanol intercalation of as-synthesized GO dramatically changes the thermal reduction behavior (i.e., the degree of oxygen removal from rGO in the presence of each alcohol in the interlayer). The absorbance spectra of GO intercalated with methanol are given in Figure 1i, and the differential spectra after annealing at 100, 175, and 200 °C are given in Figure S3, Supporting Information. In contrast to the continuous carbonyl formation (∼1650−1750 cm^{-1}) in rGO intercalated with water as shown in Figure S1, Supporting Information, the infrared absorbance remains constant during annealing (Figure 1i) after water was exchanged with methanol. The integrated total infrared absorbance (400−4000 cm^{-1}) (Figure 1iii-b) normalized to the initial total absorbance at 60 °C also confirms that there is no change in the total amount of initial oxygen (i.e., no reduction observed even after annealing at 200 °C). The carbonyl concentration calculated from the integration of peaks at 1524−1880 cm^{-1} also remains constant as shown in Figure 1iv-b after annealing at ∼200 °C. For consistency and calibration purposes, each integrated peak area is normalized to the *initial* amount of oxygen in each sample (i.e., the total integrated area of the IR spectrum).

These findings suggest that defects in reduced multilayered GO intercalated with methanol are passivated by CH_3 or C−H, presumably as a result of methanol reaction with the etch holes. There is in fact a weak C−H loss (negative peaks at 2800−3000 cm^{-1}, denoted by orange dashed lines in Figure S3, Supporting Information) and a correspondingly weak increase at ∼2900 cm^{-1} (a slight positive peak at denoted by a blue dashed line in Figure S3, Supporting Information), indicating possible H-transfer from methanol to the etch hole of rGO during annealing (consistent with the CH_x transfer from methanol molecule to the etch hole in the simulations of Figures 2 and 3).

3.4. Comparison between Methanol and Ethanol during the Thermal Reduction of GO Intercalated with Alcohols. As discussed above, water is mostly replaced by alcohols upon a 4-day immersion treatment, as evidenced by an increase of GO interlayer spacing (e.g., from ∼8.88 Å to 9.45 Å for ethanol, see Figure S2, Supporting Information). The presence of alcohol affects the thermal reduction of GO in different ways. Methanol incorporation leads to minor spectral variations during initial annealing to 100 °C, characterized mostly by little formation of C−O (1150−1320 cm^{-1}) and C═O (1700−1850 cm^{-1}) species (Figure S3, Supporting Information). In contrast, there is a substantial removal of C−O and C═O that occurs in the case of GO intercalated by ethanol (note the larger scale bar for a larger infrared absorbance in Figure S4, Supporting Information). An overall decrease in both C−O and C═O concentration is also observed in infrared absorbance spectra as shown in Figure 1ii. This decrease in both C−O and C═O concentrations during GO reduction can be explained by a different reaction mechanism between etch holes of rGO and the intercalated ethanol. It also appears that ethanol is more effective than methanol to remove intercalated water upon annealing at 175 °C (the negative peak at ∼1630 cm^{-1} in Figure S4, Supporting Information). The total integrated infrared absorbance for GO intercalated by ethanol significantly decreases as a function of annealing temperature (as normalized to the total initial absorbance at 60 °C), as shown in Figure 1iii-c. The overall decrease of the C═O concentration in Figure 1iv-c also shows the same trend for the ethanol-treated GO.

From these observations, ethanol appears to play the role of a strong reductant during thermal annealing of GO, i.e., it helps remove oxygen. In comparison, methanol intercalation does not foster the removal of oxygen, although it clearly inhibits the violent oxidization of GO (i.e., reduced concentration of new C−O and C═O formed in the etch holes) compared to the water intercalation. To gain an atomic level insight on the reduction mechanisms for oxygen removal and to understand the effect of each alcohol on the degree of reduction, we investigate the atomic scale processes of both methanol and ethanol (as atypical reductants) by performing extensive ab inito MD and DFT simulations.

3.5. MD Simulations Exploring Reactions between Methanol and a Bare Etch Hole. In alcohols, such as methanol or ethanol (Figure S6b,c, Supporting Information), hydrogen is the outermost species that is more accessible to the environment, and carbon is most stable in the center of a tetrahedral structure. The calculated bonding strengths within these alcohol molecules (shown in Figure S6b,c, Supporting Information) imply that, in both methanol and ethanol, the

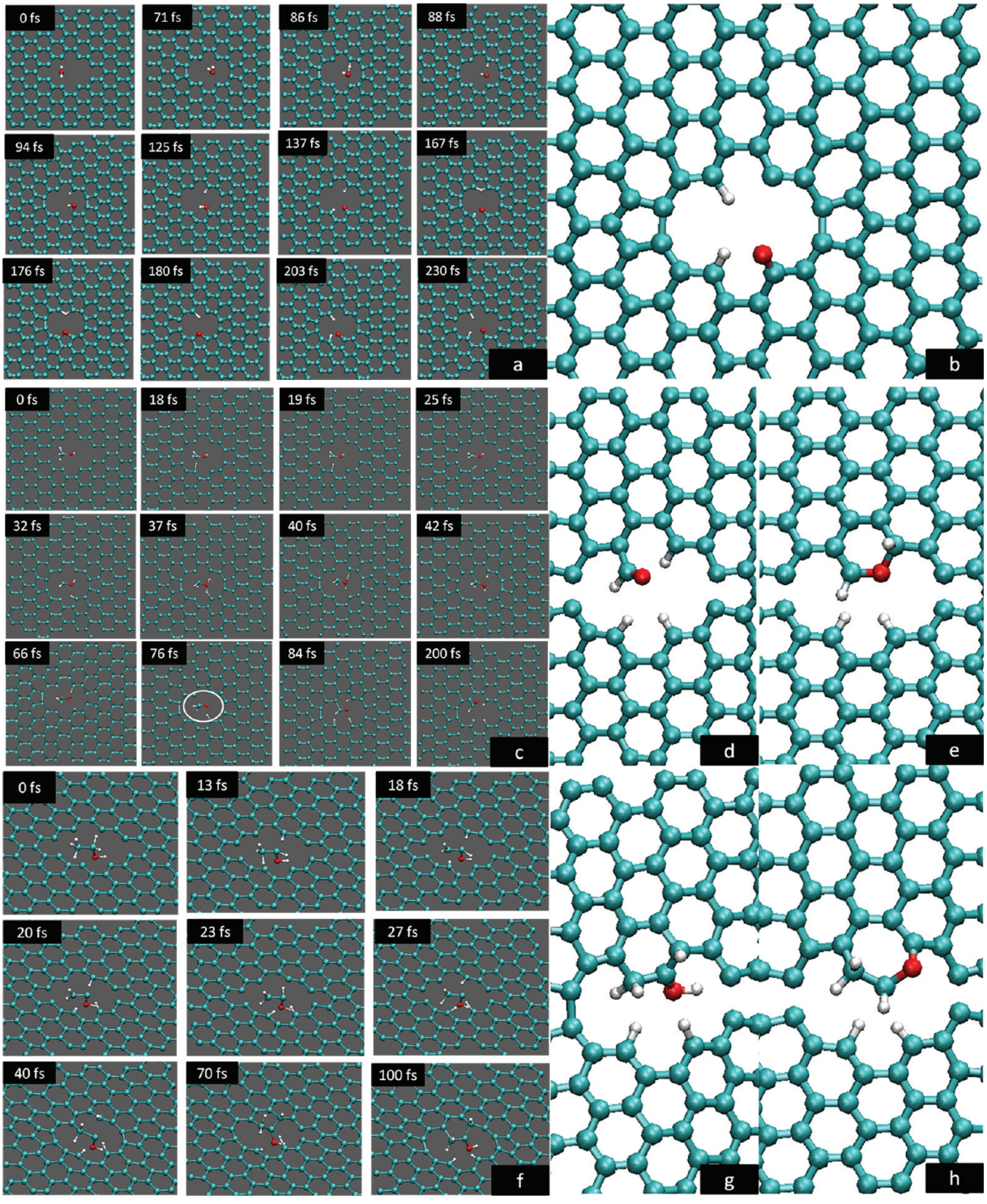

Figure 2. Intermediate snapshots of ab initio MD simulations of reactions between intercalants (water (a,b), methanol (c,e), and ethanol (f,h)) and a bare etch hole of graphene at 200 °C. All the reactions are rapid, in a time range of tens or hundreds of femtoseconds (fs). With various initial positions and orientations of intercalated molecules, carbonyl (b) is the sole result for water; carbonyl (d) and ether (e) are the two possible results observed for methanol; and hydroxyl (g) and ether (f) are the two dominant results observed for ethanol. At 1000 °C, the hydroxyl group in PANEL g is observed to evolve into a carbonyl group after a dehydrogenation process (shown in Figure S5, Supporting Information). The hydroxyl in panel g is also believed to complete its transformation to a carbonyl group easily only if there are more carbon dangling bonds available nearby.

hydrogen atoms closest to the hydroxyl groups are easiest to dissociate because the C−H bonding strength is weaker by at least 0.2−0.3 eV and 0.4−0.6 eV than other bonds in methanol and ethanol, respectively. Also, the incidence configuration of the alcohol molecules into the etch holes (i.e., the relative positions and orientations of alcohol molecules with respect to the etch holes) can affect the reaction probability and pathways.

Ab initio MD simulations verify that the reactions are initiated by a hydrogen transfer from methanol or ethanol into the bare etch hole in rGO during annealing (see Figure 2c,f).

dx.doi.org/10.1021/jp212584t | J. Phys. Chem. C 2012, 116, 9969−9979

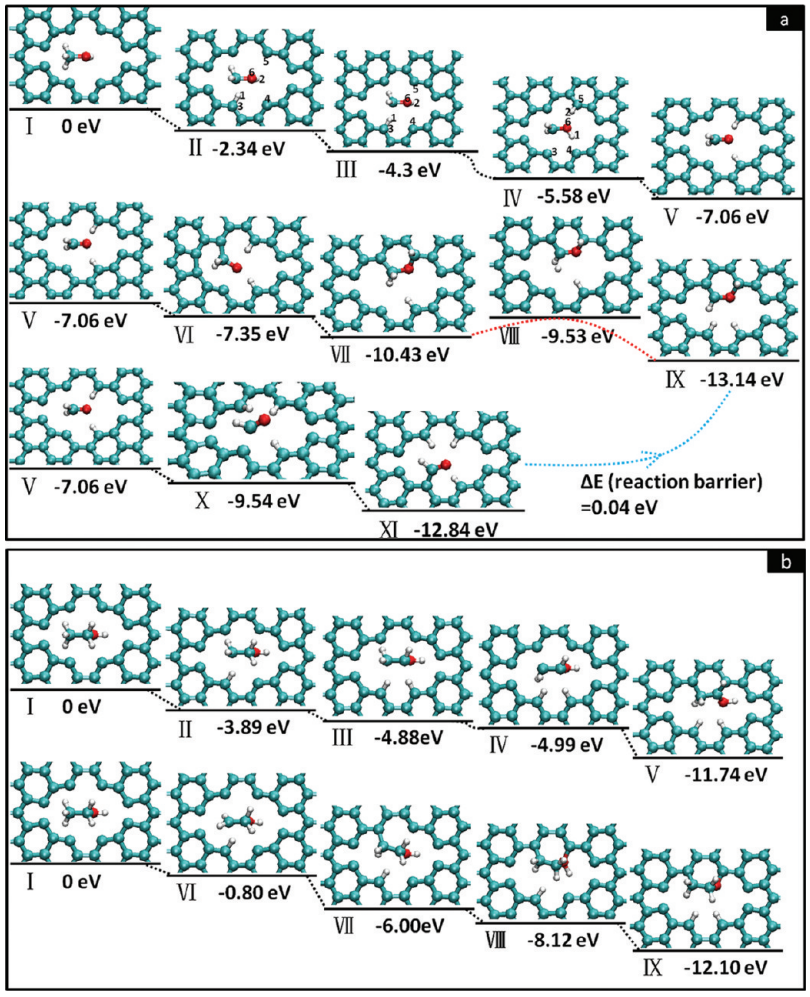

Figure 3. Reaction pathways of a bare etch hole and alcohols (methanol (a) and ethanol (b)). Black dashed line means a direct reaction without barriers. The black dashed curves in III–IV of both panels a and b represent an adjustment of structures (e.g., rotation of fragments) rather than reaction.

We have performed a series of calculations using a number of initial structures with the alcohol molecules staying around the center of bare etch holes within 5 Å from the GO basal plane, at mainly two temperatures: 200 and 1000 °C. Calculations are performed at 1000 °C, in addition to 200 °C, to test the stability of the products. Among all these simulated reactions, two main reactions are observed upon methanol decomposition at the bare etch hole of the rGO: (1) formation of a new etch hole carbonyl as shown in Figure 2d and (2) formation of an etch hole ether shown in Figure 2e. The final product is determined by the initial specific relative position of the methanol to the etch hole. These simulations indicate that the etch hole carbonyls or ethers stabilize the etch holes of rGO until another out-of-plane hydroxyl or epoxide group approaches the etch hole to produce CO_2 and etch hole edge dangling bonds. In contrast to water intercalation, however, the loss of carbon from rGO in the form of CO_2 is compensated by carbon addition from methanol decomposition. Since the etch holes are not enlarged in methanol intercalation, carbon dangling bond concentration is preserved and further formation of etch hole carbonyls and ethers is inhibited. Therefore, as evidenced from IR studies, an almost constant concentration of carbonyls is observed for methanol intercalation (Figure 1iv-b), compared with a substantially large carbonyl concentration increase for water intercalation (Figure 1iv-a).

Examining the detailed reaction pathway in Figure 2c reveals that dehydrogenation of methanol by carbon dangling bonds at the etch holes is the critical reaction step. In a snapshot of 76 fs shown in Figure 2c, a formaldehyde (H–C═O–H) species is formed as an intermediate product before the carbon is captured by the reactive etch holes. This observation explains the recent finding of GO acting as an oxidizing catalyst for the transformation of alcohols to aldehydes or ketones, as reported by Dreyer et al.,[35] particularly above 100 °C. Our experimental finding shows that the largest amount of CO_2 production is observed after ∼100 °C anneal as given in the inset of Figure S1b, Supporting Information. Our simulation results clearly indicate that the catalytic activity of as-synthesized GO is correlated with the formation of etch holes in rGO, which behave as the active sites.

3.6. MD Simulations Exploring the Reactions between Ethanol and a Bare Etch Hole. Compared to methanol, ethanol not only has a potential sp^2 C═C bonding in its structure upon the removal of a hydrogen atom from each carbon but also has intrinsically a higher C/O ratio (2:1) than that (1:1) of methanol. Both of these characteristics are important to account for the healing capability of ethanol upon reaction with etch holes of rGO. The most frequently observed MD simulation event, shown in Figure 2f, indicates that a double-carbon fragment (CH_2CHOH) is an important

dx.doi.org/10.1021/jp212584t | J. Phys. Chem. C 2012, 116, 9969–9979

intermediate byproduct, which is subsequently grafted onto the etch hole dangling carbons. In this reaction involving ethanol, two carbon atoms are incorporated into the hexagonal bonding network as shown in Figure 2g. A new hexagonal carbon ring is formed, and the graphitic structure of rGO is effectively restored. The remaining hydroxyls in Figure 2g can be easily transformed to carbonyls at higher temperatures (e.g., 1000 °C as shown in Figure S5b, Supporting Information). In our etch hole model, there is only a small number of dangling carbons, and it can be reasonably inferred that, even at 200 °C, the hydroxyl in Figure 2g can be easily transformed into a carbonyl (like the process from Figure 2a, 125 fs to 137 fs in the water case) when there are many neighboring dangling carbons to accommodate the hydrogen transferred from hydroxyl. This type of hydroxyl-to-carbonyl transformation occurs with an almost negligible (~0.1 eV) activation energy as previously shown.[33] The formation of etch hole ether is another frequently observed event in MD simulations, as shown in Figure 2h. Consequently, as with methanol, etch hole hydroxyls (or carbonyls) and ethers are formed during the thermal annealing of rGO intercalated by ethanol.

In summary, we find that ethanol does not participate in the reduction reactions as a typical reductant but provides instead additional carbon atoms to repair etch holes. Ethanol can effectively contribute to the reduction and increased graphitization of rGO because it prevents basal plane epoxides and hydroxyls to oxidize and enlarge the defect sites.

3.7. Reaction Energy Profiles between Alcohols and a Bare Etch Hole. DFT total energy calculations shown in Figure 3 are carried out to examine the main reaction pathways identified by the MD simulations. Since the bare etch hole with carbon dangling bonds is extremely reactive, both methanol and ethanol are shown to decompose at a bare etch hole of rGO without any activation barriers.

It is worthwhile to examine the methodologies used in computing these pathways for such strong reactions. Unlike common reactions that need thermal activation to proceed or catalysts to lower the reaction barriers, there are no reaction barriers in the spontaneous reactions considered here. Thermal annealing is only applied in this experiment to remove the oxygen and to form etch holes. Once bare etch holes are formed, the reaction between intercalated alcohol molecules and a number of carbon dangling bonds is extremely strong (i.e., no reaction barrier). In order to sort out the possible intermediate structures in such reactions and to quantify the existence and magnitude of reaction barriers, alcohol and its various fragments in the process of the reactions are fixed, for the energy calculations, in intermediate positions that are not metastable, but etch hole structures are still allowed to relax to investigate the interaction between the etch hole and the alcohol (or its fragments). Since the fixed structures are known to have higher energies than those of optimized intermediate structures, the absence of reaction barriers for the fixed intermediate configurations implies that there are no reaction barriers in realistic reactions.

We focus on explaining some detailed configurations and energy data in these reaction pathways:

(1) Configuration III in Figure 3a is an intermediate structure obtained as one hydrogen is transferred to the available dangling bond of an etch hole carbon (carbon 3 in Figure 3a). To determine whether there is a transition barrier for this overall process, the nudged elastic band (NEB) method is applied between configuration I and configuration III. Configuration II is obtained as a saddle point with no activation barrier, and the energy difference between configurations II and III is large (~2 eV) because of strong stabilization (interaction) of the OH group of the fragment (H_2COH) with the carbon 5 in the etch hole.

(2) In Figure 3a III–IV (connected by a black dashed curve), the hydrogen 1 is transferred manually from dangling carbon 3 to dangling carbon 5 for the calculations. The detailed transfer process can be found in the molecular dynamic scenario depicted in Figure 2c, from 19 fs to 40 fs. In this scenario, hydrogen 1 (atom indices are shown in Figure 3a) hops from carbon 3 to carbon 4, and then hydrogen 1 transfers from carbon 4 to oxygen 6, while hydrogen 2 transfers from oxygen 6 to carbon 5). This dynamic process also results in a hydrogen transfer from carbon 3 to carbon 5. The overall process occurs extremely fast without energy barriers, as indicated by the completion time in MD simulation (~21 fs) and the descent net energy drop in DFT total energy calculation (~1.28 eV energy difference between configuration III and configuration IV).

(3) Significant energy drops in hydrogen transfer reactions of Figure 3a I–II (ΔE = −2.34 eV), IV–V (ΔE = −1.48 eV), VII–IX (ΔE = −2.71 eV), and V–X (ΔE = −2.48 eV) and Figure 3b I–II (ΔE = −3.89 eV) and VIII–IX (ΔE = −3.98 eV) indicate that there are different hydrogen bonding strengths at different carbon sites. Furthermore, the C–H bond strength is believed to only weakly depend on the chemical environment, typically of order 0.8 eV as shown in Figure 3b I–VI for a simple H transfer. In contrast, the large energy drops in the above reactions (mostly 2–4 eV) largely result from (i) a hydrogen atom transfer to a more stable energy state; (ii) an etch hole configuration relaxation (and adjustment) after hydrogen transfer; (iii) an adjustment of the relative positions between alcohol fragments and etch holes leading to more stable configurations; and (iv) the formation of new final state structures (either etch hole carbonyl or ether incorporation). Note that the final energies of both etch hole carbonyl and ether are very close to each other (e.g., the energy difference is 0.04 eV) as shown in Figure 3a IX and XI, and furthermore, their mutual transformation is also quite possible from an energetic point of view.

Both Figure 3a,b show the detailed processes of methanol or ethanol reacting with a bare etch hole of rGO, in which two types of reactions dominate: hydrogen transfer and carbon incorporation. When an alcohol molecule approaches a bare etch hole, hydrogen transfer occurs from the alcohol molecule to a carbon dangling bond, resulting in a byproduct formation. After this dehydrogenation process, the central carbon atom in the tetrahedral structure of the alcohol molecule can be incorporated into the etch hole, as a part of a byproduct that directly interacts with the bare etch hole. For example, the formation of formaldehyde (Figure 3a-V) results from two sequential hydrogen transfers into the etch hole, and this byproduct is readily incorporated into the carbon network as shown in Figure 3a VI–IX. In this example, there is the addition of one carbon (from the formaldehyde) to the etch hole carbon dangling bonds. Such a process supports the

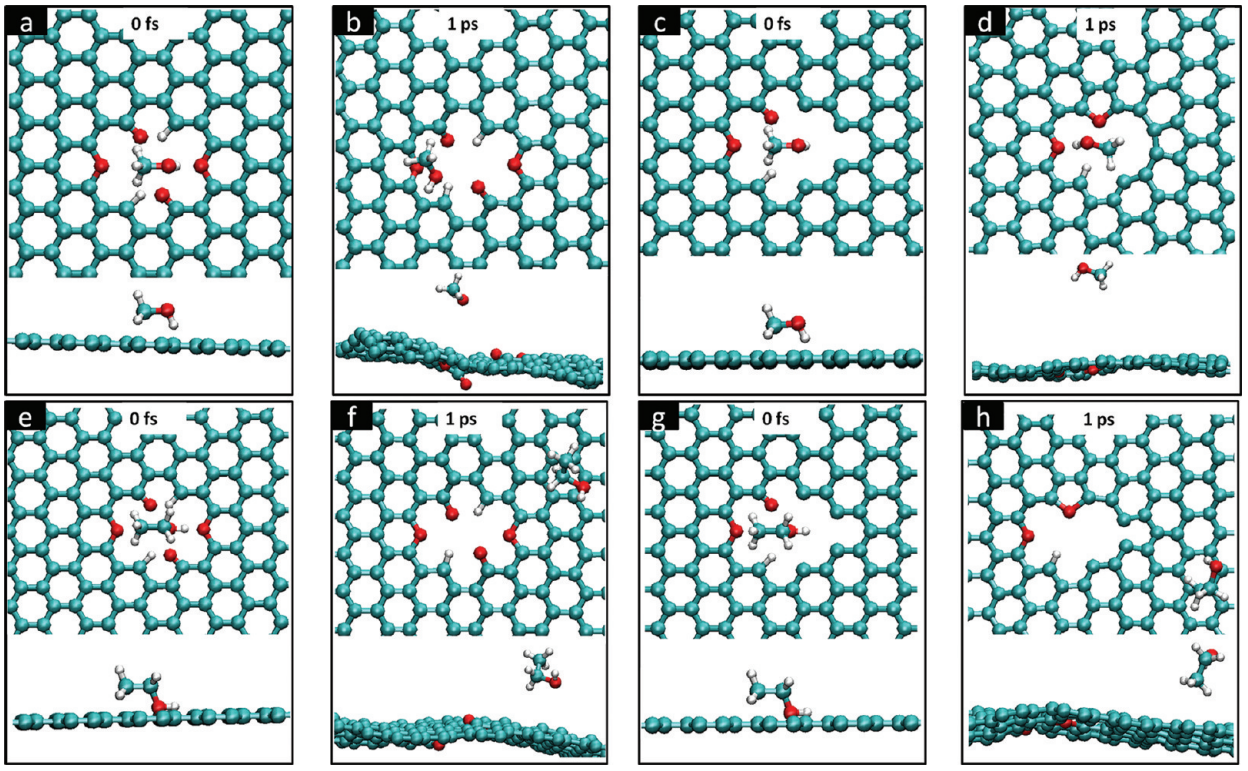

Figure 4. MD simulations of the possible interactions between a methanol molecule and a fully saturated etch hole (a,b) and a partially passivated etch hole (c,d) and between an ethanol molecule and a fully saturated etch hole (e,f) and a partially passivated etch hole (g,h) at 200 °C. The top panel in each figure is a top view, and the bottom panel is a side view.

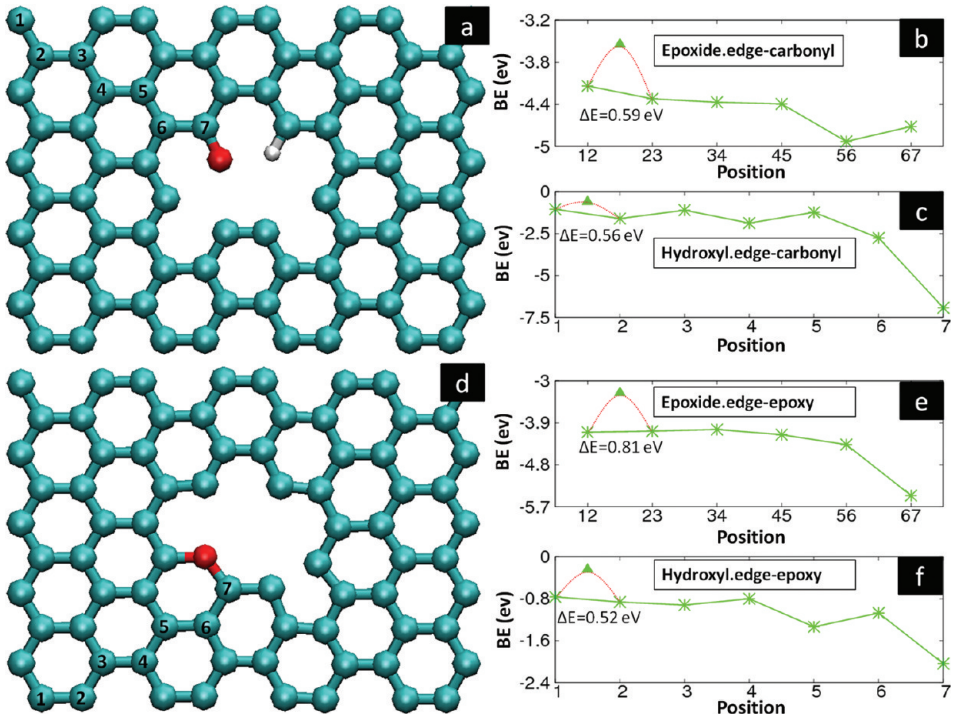

Figure 5. Epoxide (b,e) and hydroxyl (c,f) adsorbed on different positions nearby an etch hole decorated by carbonyl (a) and ether (d). The red dashed curves in panels b, c, e, and f show the hopping barriers of epoxide and hydroxyl on the graphene basal plane away from the etch hole.

inference from the data in Figure 1 iii,iv that the etch hole size remains constant upon annealing. The mechanism in Figure 3a explains how the incorporation of a carbon atom from methanol into the carbon network can compensate for the carbon removed by the oxidation reaction (producing CO or CO_2).

Figure 3b shows a similar reaction pathway for the ethanol reaction with the bare etch hole. Through a sequence of

dx.doi.org/10.1021/jp212584t | J. Phys. Chem. C 2012, 116, 9969–9979

hydrogen transfer reactions, the carbon atoms in the ethanol molecule are able to form C−C bonds with the bare etch hole. Figures 3b, V and IX, shows the C−C−O ethanol backbone structure incorporates into the grapheme bonding network. Therefore, while the reactions of methanol and ethanol both lead to the incorporation of carbon, ethanol can add two carbon atoms to the etch hole, thus completing the hexagonal bonding and repairing the etch hole. This conclusion is consistent with the experimental observations in Figure 1iii,iv.

3.8. Alcohol Interactions with Fully and Partially Saturated Etch Holes. In the thermal annealing study of GO intercalated by alcohols, a model bare etch hole was constructed by removing eight neighboring carbon atoms with unpassivated carbon dangling bonds, thus leaving enough space and active sites for the addition of a methanol or ethanol. It is, however, more likely that dangling bonds are generated sequentially at the etch hole edges. It is therefore relevant to simulate methanol or ethanol reactions with *partially* (Figure 4c,d;g,h) and *fully* (Figure 4a,b;e,f) saturated etch holes to determine whether reactions are still possible.

A partially saturated etch hole is modeled without neighboring carbon dangling bonds, and both ether and carbonyl groups are included in our model (Figures 4c,d;g,h). As a result, both methanol and ethanol are repelled away from the etch hole region during long simulation times (~1 ps). Spontaneous chemical reactions are therefore not possible between alcohol molecules and the partially or fully saturated etch holes in which there are only isolated carbon dangling bonds or none at all. Therefore, there is a need for adjacent carbon dangling bonds, which can be produced sequentially by reduction reactions at etch holes. These results highlight the importance of developing transient bare etch holes with adjacent carbon dangling bonds during the annealing process for an efficient graphitization of rGO by ethanol.

3.9. Adsorption and Diffusion of Hydroxyl/Epoxide on Graphene Basal Plane to Oxygen-Decorated Etch Holes. After the reaction between the etch holes of rGO and ethanol, etch hole ethers or carbonyls are formed. Figure 5b,c,e,f shows that out-of-plane hydroxyl/epoxide groups have an affinity for etch hole sites (either carbonyl-decorated or ether-decorated), which is indicated by a negative binding energy at etch hole sites relative to that away from etch hole sites. The hopping barriers of out-of-plane hydroxyl/epoxide groups (~0.5−0.8 eV) between neighboring adsorption sites on graphene basal plane is reasonably small and easily overcome at experimental temperatures and time scales. When out-of-plane hydroxyls/epoxides get close to the etch hole oxygen-decorated groups, CO_2 is released,[36−38] and bare etch holes are formed with dangling carbon bonds (i.e., reopening of the etch hole hexagonal rings). Through these reactions, carbon dangling bonds are formed, and highly efficient reduction and graphitization of GO is subsequently activated with the aid of thermal annealing and ethanol intercalation.

3.10. Discussions on Larger Alcohol Molecules and Ethylene. With present dangling carbon bonds upon formation, the etch holes are highly reactive. The intrinsic differences of the chemical reactivity and stability among different alcohols are therefore less important than the size differences of the alcohol molecules. The larger alcohol molecules, with 3 or more carbon atoms and correspondingly more hydrogen atoms, require a larger space to react with an etch hole and therefore are expected to be able to heal small holes. Temperature was shown to be a critical factor in the formation and enlargement of the etch holes in rGO, and also for the diffusion of the alcohol molecules within the interlayer of rGO. Therefore, the interaction between large alcohol molecules and rGO is expected to require higher temperatures than for smaller molecules. Furthermore, large alcohol molecules are not as flexible as small molecules like ethanol and may therefore have more difficulty in repairing small etch holes with irregular shapes. These considerations suggest that ethanol is a mobile molecule that can efficiently repair etch holes of GO at mild temperatures. However, if aqueous GO is dispersed within the alcohol solutions during annealing, the situation is different because the concentration is never depleted. In this case, as recently shown,[25] isopropanol and benzyl alcohol are significantly more efficient than ethanol in reducing GO. In general, more work is needed to evaluate the effects of a variety of large alcohol molecules in different experimental conditions.

Ethylene, with an sp^2 C═C structure and an infinite C/O ratio (no oxygen content), may be intuitively expected to be more efficient in the graphitization of GO upon annealing. The total energy calculations shown in Figure 6a−c confirms that ethylene is able to decompose and incorporate into bare etch holes. However, MD simulations at 200 °C show that hydrogen transfer with the formation of an acetylene molecule is the only observable event during the simulation time of 2 ps. Graphitization resulting from carbon incorporation into the bare etch hole of rGO is not observed. This can be easily

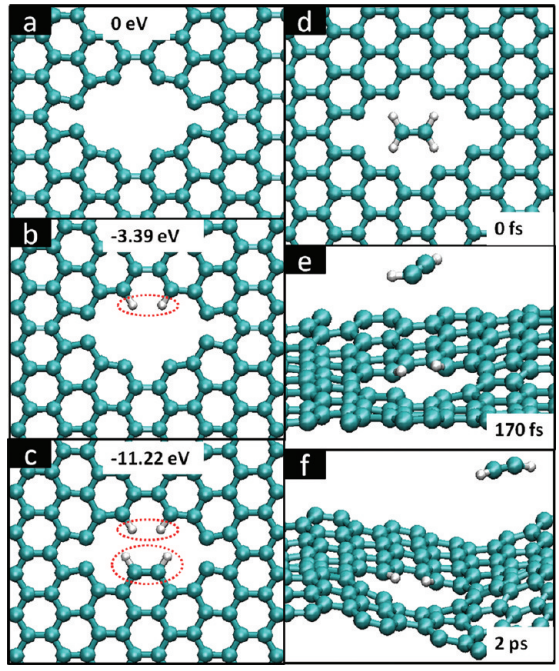

Figure 6. DFT (a−c) and MD (d−f) calculations of the possible interactions between an ethylene molecule and a bare etch hole in rGO. The reference energy is 0 eV (a) for a bare etch hole plus a free ethylene molecule; −3.39 eV is the relative energy of the structure shown in panel b plus an acetylene (C_2H_2) molecule; −11.22 eV is the relative energy of the structure shown in panel c, where the ethylene molecule is totally incorporated into the bare etch hole. (d−f) Simulated kinetic process of the interaction between a bare etch hole and an acetylene molecule nearby. Although a energetic sketch (a−c) reveals a possibility of ethylene incorporation into a bare etch hole, the kinetic evolution is rejected in the MD simulation, suggesting the presence of large activation energy barriers.

dx.doi.org/10.1021/jp212584t | J. Phys. Chem. C 2012, 116, 9969−9979

understood since etch holes in rGO are hydrophilic and do not have strong affinity to ethylene molecules. We therefore speculate that ethylene is not as good as ethanol for the graphitization of GO. Indeed, López et al. reported that, while ethylene provides an efficient carbon source to repair of GO during chemical vapor deposition (CVD) growth,[39] higher temperatures (~800 °C) are needed. Lower temperatures resulted in samples of unaltered conductivities, indicating that ethylene is less efficient than ethanol that reacts at ~200 °C. They also cautioned that temperatures higher than 800 °C led to complete degradation of the rGO layers. The healing mechanism reported by López is consistent with conventional CVD growth taking place in relatively harsh conditions.

In our experiment, the dangling bonds around the etch hole periphery in rGO, created upon CO_2 or CO formation, help the decomposition of alcohol molecules and the formation of a new hexagonal ring. With ethanol, for each carbon removed, two new carbon atoms are incorporated, thus slowly healing the structure. In contrast, if an ethylene molecule were to incorporate into a bare etch hole (although that is energetically favorable, as shown in Figure 6a−c, from DFT calculations), the edge holes would be hydrogen-terminated, which would prevent further ring formation since CO_2 (i.e., dangling bonds) cannot be formed, thus blocking the graphitization channel. In summary, the oxygen-containing groups at the etch holes of rGO are necessary for the reopening of etch hole hexagonal rings that are critical for further reactions including graphitization with ethanol.

4. CONCLUSIONS

A combination of experimental and theoretical studies has shown that ethanol is superior over methanol for the reduction and graphitization of GO during thermal annealing. The formation of etch holes in rGO and transient carbon dangling bonds during annealing (upon CO_2 release) is essential for reactions between rGO and alcohol molecules (e.g., methanol and ethanol). When ethanol is decomposed and integrated into the etch hole of rGO, a new hexagonal carbon ring is formed with the attachment of oxygen-containing groups like carbonyls and ethers. These etch hole oxygen-decorated groups react with other oxygen-containing groups in close proximity and reopen the ring for further carbon incorporation leading to an improved graphitization of rGO. The elucidation of atomic scale mechanisms of improved reduction and graphitization of GO by ethanol in this work provides guidance for rational experimental designs of GO reduction and graphitization. Furthermore, it also provides insight on the recently explored oxidizing catalytic functions of thermal rGO. These findings suggest new ways to tailor the structural and electronic properties of rGO and graphene for a variety of applications requiring defect engineering.

■ ASSOCIATED CONTENT

Supporting Information

FTIR absorbance spectra for GO intercalated with water annealed at the temperature range of 60−200 °C; FTIR differential spectra for GO intercalated with methanol and ethanol annealed at the temperature range of 60−200 °C; XRD patterns of GO intercalated with water, methanol, and ethanol, respectively; MD simulations of 1000 °C annealing of GO intercalated with ethanol; schematics of molecule structures and calculated bonding strengths for water, methanol, and ethanol; discussion on larger size alcohols. This material is available free of charge via the Internet at http://pubs.acs.org.

■ AUTHOR INFORMATION

Corresponding Author

*E-mail: kjcho@utdallas.edu (K.C.); chabal@utdallas.edu (Y.C.).

Present Address

[‖]Department of Therapeutic Radiology, Yale School of Medicine, Yale University, New Haven, Connecticut 06520, United States.

Author Contributions

C.G. carried out all the density functional theory and ab initio molecular dynamics calculations. M.A. carried out experiments related to the synthesis of GO and alcohol-intercalated GO, thermal reduction studies combined with FTIR measurements, and XRD analyses. K.C. and Y.C. directed and supervised the theoretical and experimental research, respectively. C.G., M.A., Y.C, and K.C. contributed to the article. R.M.A. preformed Reax-FF molecular dynamics simulations in the early stage of this project. All authors discussed the experimental and simulation results.

Notes

The authors declare no competing financial interest.

■ ACKNOWLEDGMENTS

We thank the support from Texas Advanced Computing Center (TACC) for computer resources. M.A. was fully supported by U.S. Department of Energy, Office of Basic Energy Sciences, Division of Materials Sciences and Engineering under Award DE-SC001951, and C.G. was partly supported by NSF (CHE-0911197) and The Texas Higher Education Coordination Board (NHARP).

■ REFERENCES

(1) Novoselov, K. S.; Geim, A. K.; Morozov, S. V.; Jiang, D.; Zhang, Y.; Dubonos, S. V.; Grigorieva, I. V.; Firsov, A. A. *Science* **2004**, *306*, 666−669.

(2) Berger, C.; Song, Z.; Li, T.; Li, X.; Ogbazghi, A. Y.; Feng, R.; Dai, Z.; Marchenkov, A. N.; Conrad, E. H.; First, P. N.; et al. *J. Phys. Chem. B* **2004**, *108*, 19912−19916.

(3) Yu, Q.; Lian, J.; Siriponglert, S.; Li, H.; Chen, Y. P.; Pei, S.-S. *Appl. Phys. Lett.* **2008**, *93*, 113103.

(4) N'Diaye, A. T.; Bleikamp, S.; Feibelman, P. J.; Michely, T. *Phys. Rev. Lett.* **2006**, *97*, 215501.

(5) Li, X.; Cai, W.; An, J. H.; Kim, S.; Nah, J.; Yang, D.; Piner, R.; Velamakanni, A.; Jung, I.; Tutuc, E.; et al. *Science* **2009**, *324*, 1312−1314.

(6) Bae, S.; Kim, H.; Lee, Y.; Xu, X.; Park, J.-S.; Zheng, Y.; Balakrishnan, J.; Lei, T.; Kim, H. R.; Song, Y., II; et al. *Nat. Nanotechnol.* **2010**, *5*, 574−578.

(7) Loh, K. P.; Bao, Q.; Eda, G.; Chhowalla, M. *Nat. Chem.* **2010**, *2*, 1015−1024.

(8) Eda, G.; Chhowalla, M. *Adv. Mater.* **2010**, *22*, 2392−2415.

(9) Gómez-Navarro, C.; Meyer, J. C.; Sundaram, R. S.; Chuvilin, A.; Kurasch, S.; Burghard, M.; Kern, K.; Kaiser, U. *Nano Lett.* **2010**, *10*, 1144−1148.

(10) Lu, G.; Park, S.; Yu, K.; Ruoff, R. S.; Ocola, L. E.; Rosenmann, D.; Chen, J. *ACS Nano* **2011**, *5*, 1154−1164.

(11) Acik, M.; Lee, G.; Mattevi, C.; Chhowalla, M.; Cho, K.; Chabal, Y. J. *Nat. Mater.* **2010**, *9*, 840−845.

(12) Bagri, A.; Grantab, R.; Medhekar, N. V.; Shenoy, V. B. *J. Phys. Chem. C* **2010**, *114*, 12053−12061.

(13) Cai, W.; Piner, R. D.; Stadermann, F. J.; Park, S.; Shaibat, M. A.; Ishii, Y.; Yang, D.; Velamakanni, A.; An, S. J.; Stoller, M.; et al. *Science* **2008**, *321*, 1815−1817.
(14) Yan, J.-A.; Xian, L.; Chou, M. Y. *Phys. Rev. Lett.* **2009**, *103*, 086802.
(15) Tung, V. C.; Allen, M. J.; Yang, Y.; Kaner, R. B. *Nat. Nanotechnol.* **2009**, *4*, 25−29.
(16) Stankovich, S.; Dikin, D. A.; Piner, R. D.; Kohlhaas, K. A.; Kleinhammes, A.; Jia, Y.; Wu, Y.; Nguyen, S. T.; Ruoff, R. S. *Carbon* **2007**, *45*, 1558−1565.
(17) Si, Y.; Samulski, E. T. *Nano Lett.* **2008**, *8*, 1679−1682.
(18) Shin, H.-J.; Kim, K. K.; Benayad, A.; Yoon, S.-M.; Park, H. K.; Jung, I.-S.; Jin, M. H.; Jeong, H.-K.; Kim, J. M.; Choi, J.-Y.; et al. *Adv. Funct. Mater.* **2009**, *19*, 1987−1992.
(19) Wang, G.; Yang, J.; Park, J.; Gou, X.; Wang, B.; Liu, H.; Yao, J. *J. Phys. Chem. C* **2008**, *112*, 8192−8195.
(20) Fernández-Merino, M. J.; Guardia, L.; Paredes, J. I.; Villar-Rodil, S.; Solís-Fernández, P.; Martínez-Alonso, A.; Tascón, J. M. D. *J. Phys. Chem. C* **2010**, *114*, 6426−6432.
(21) Dreyer, D. R.; Park, S.; Bielawski, C. W.; Ruoff, R. S. *Chem. Soc. Rev.* **2010**, *39*, 228−240.
(22) Park, S.; Ruoff, R. S. *Nat. Nanotechnol.* **2009**, *4*, 217−224.
(23) Gao, X.; Jang, J.; Nagase, S. *J. Phys. Chem. C* **2010**, *114*, 832−842.
(24) Gao, W.; Alemany, L. B.; Ci, L.; Ajayan, P. M. *Nat. Chem.* **2009**, *1*, 403−408.
(25) Dreyer, D. R.; Murali, S.; Zhu, Y.; Ruoff, R. S.; Bielawski, C. W. *J. Mater. Chem.* **2011**, *21*, 3443−3447.
(26) Su, C.-Y.; Xu, Y.; Zhang, W.; Zhao, J.; Liu, A.; Tang, X.; Tsai, C.-H.; Huang, Y.; Li, L.-J. *ACS Nano* **2010**, *4*, 5285−5292.
(27) Park, S.; An, J.; Potts, J. R.; Velamakanni, A.; Shanthi, M.; Ruoff, R. S. *Carbon* **2011**, *49*, 3019−3023.
(28) Hummers, W. S.; Offeman, R. E. *J. Am. Chem. Soc.* **1958**, *80*, 1339−1339.
(29) Gilje, S.; Han, S.; Wang, M.; Wang, K. L.; Kaner, R. B. *Nano Lett.* **2007**, *7*, 3394−3398.
(30) Kresse, G.; Furthmüller, J. *J. Comput. Mater. Sci.* **1996**, *6*, 15−50.
(31) Blöchl, P. E. *Phys. Rev. B* **1994**, *50*, 17953−17979.
(32) Perdew, J.; Burke, K.; Ernzerhof, M. *Phys. Rev. Lett.* **1996**, *77*, 3865−3868.
(33) Acik, M.; Mattevi, C.; Gong, C.; Lee, G.; Cho, K.; Chhowalla, M.; Chabal, Y. J. *ACS Nano* **2010**, *4*, 5861−5868.
(34) Li, J.-L.; Kudin, K. N.; McAllister, M. J.; Prud'homme, R. K.; Aksay, I. A.; Car, R. *Phys. Rev. Lett.* **2006**, *96*, 176101.
(35) Dreyer, D. R.; Jia, H.-P.; Bielawski, C. W. *Angew. Chem., Int. Ed.* **2010**, *49*, 6813−6816.
(36) Bagri, A.; Mattevi, C.; Acik, M.; Chabal, Y. J.; Chhowalla, M.; Shenoy, V. B. *Nat. Chem.* **2010**, *2*, 581−587.
(37) Radovic, L. R. *J. Am. Chem. Soc.* **2009**, *131*, 17166−17175.
(38) Sun, T.; Fabris, S.; Baroni, S. *J. Phys. Chem. C* **2011**, *115*, 4730−4737.
(39) López, V.; Sundaram, R. S.; Gómez-Navarro, C.; Olea, D.; Burghard, M.; Gómez-Herrero, J.; Zamora, F.; Kern, K. *Adv. Mater.* **2009**, *21*, 4683−4686.